Theory for enzymatic degradation of semi-crystalline polymer particles

Michael Schindler* and Ludwik Leibler
Gulliver, École Supérieure de Physique et Chimie Industrielles, Paris Sciences et Lettres Université, CNRS, Paris 75005, France

Hernan Garate
Gulliver, École Supérieure de Physique et Chimie Industrielles, Paris Sciences et Lettres Université, CNRS, Paris 75005, France and Laboratoire Sciences et Ingénierie de la Matière Molle, École Supérieure de Physique et Chimie Industrielles, Paris Sciences et Lettres Université, Sorbonne Université, CNRS, Paris 75005, France

(Dated: January 20, 2026)

In enzymatic recycling or biodegradation of semi-crystalline plastic waste, crystalline spherulites embedded into an amorphous matrix hinder and slow down depolymerisation. When the enzymatic depolymerisation temperature exceeds the glass transition temperature, these spherulites tend to grow. The depolymerisation process is thus controlled by a competition between erosion of the amorphous matrix from the particle surface and the growth of recalcitrant spherulites within the particle bulk and at its surface. We present a geometric model that captures this competition, together with an algorithm to solve the equations numerically. Our algorithm introduces a new extension of Voronoi/Delaunay tessellation in space. We extract the parameters for the model from experimental data on the enzymatic depolymerization by hydrolase LCC-ICCG of PET bottle flakes and textile waste, in order to make a prediction of the observed degradation yield as a function of time. Both the final yield and the degradation kinetics are correctly predicted. Most importantly, the model clarifies how and to which extent nucleating agents, impurities, additives, and/or rapid crystal growth present in the waste can undermine pretreatment efforts aiming to initiate depolymerisation from a material with a low initial crystallinity.

This document is the unedited author's version of a submitted manuscript subsequently accepted for publication in 'Macromolecules'. To access the final published article, see `https://doi.org/10.1021/acs.macromol.5c03444`.

I. INTRODUCTION

Enzymatic depolymerization of plastics has emerged as a promising route to enable a circular economy for polymeric materials [1–8]. By operating under mild, aqueous conditions and exhibiting high selectivity, enzymes offer a more sustainable alternative to conventional chemical recycling processes [9]. In typical processes, plastic material is mechanically broken (milled) into particles of the size of a few hundred micrometers. These particles are then dispersed in water and brought into contact with an enzyme, which adsorbs onto the particle surface and catalyzes successive bond-cleavage reactions that gradually erode the particle. As depolymerization progresses, soluble monomers or oligomers are released into the medium. Enzymes capable of cleaving the backbones of multiple classes of semi-crystalline polymers, including polyesters [10], polyamides [11], and certain polyurethanes [12], establish biocatalysis as a powerful strategy for plastic recycling.

Enzymatic depolymerization requires sufficient polymer chain mobility, making reaction temperature a critical parameter. Depolymerization is most effective at temperatures above the polymer's glass transition temperature (T_g) and below its crystallisation temperature (T_c). The optimal temperature depends on the polymer: Poly(ethylene terephthalate) (PET) is typically depolymerised around 65–70°C [1, 2, 9] whereas aliphatic polyesters with T_g well below room temperature, such as poly(ϵ-caprolactone) and poly(1, 4-butylene adipate), can be efficiently degraded at milder temperatures (30–40°C) [13–16].

A key feature of most commodity or high performance engineering plastics is their semi-crystalline nature, deliberately controlled during synthesis and processing [17, 18], in order to achieve desirable properties such as mechanical strength and dimensional stability [19], gas barrier performance, and chemical resistance [20]. Crystallinity, while crucial for performance, reduces susceptibility to enzymatic depolymerization: amorphous domains are amenable to enzyme-catalyzed chain scission, whereas crystalline regions are densely packed and energetically unfavorable for bond cleavage, making them recalcitrant [1, 6, 16, 21].

The crystallinity problem can be mitigated for polymers that crystallise slowly, such as PET or PLA, by an additional pretreatment step before milling. If the plastic particles are melted and rapidly cooled (quenched) before milling, then they will be mostly amorphous. The cooling conditions (e.g. melt temperature, cooling rate or cool-

* michael.schindler@espci.fr

ing bath temperature) and polymer molecular parameters will determine the residual degree of crystallinity and crystallite organisation and morphology. A material made of shorter chains, which crystallise faster than longer chains, exhibits a higher degree of crystallinity after quenching under identical conditions. Additionally, real plastic waste streams contain an uncontrolled number of nucleating agents, as well as other additives such as catalysts, plasticisers, dyes, pigments, impact modifiers, or fillers, which favour nucleation and crystal growth. For such highly formulated wastes amorphization by fast melt cooling pretreatment is more challenging and less efficient than for model polymers or less formulated or contaminated wastes such as PET bottles [22].

The pretreatment by melting and milling serves as a starting point for the enzymatic depolymerization. The reaction temperature is above T_g and below T_c, such that any of the mentioned impurities or preexisting spherulites inside the otherwise quenched amorphous matrix tend to grow, forming partly crystalline spherulites which grow and coalesce [23]. Their growth rate depends on how close the reaction bath temperature is to T_g and to T_c. The number of spherulites and thus also their distance is determined by the density of the nucleating impurities or the density of preexisting spherulites. What follows is a competition between spherulite growth (partial crystallisation) and degradation of amorphous matrix in the reaction bath. It is one of the aims of the theory presented here to predict how the depolymerization kinetics and reaction yield will depend on the starting crystalline structure.

The role of initial crystallinity and of its evolution in the reaction bath in plastics degradation has mainly been investigated in terms of the overall crystallinity degree [24–29]. There are only few experimental studies [28, 30], and we are aware of one model [31], which consider also the morphology of the materials while degrading.

Beyond the overall crystallinity, the morphology of the spherulites and their growth dynamics plays a decisive role for the quantitative outcome of the degradation process. Figure 1 visualises the concept: The same volume of crystalline material is distributed into different numbers of spherulites. They have the same crystallinity degree, but they will evolve differently during depolymerization. Even if the spherulites grow at the same rate, it is visually evident that the many small ones are closer to each other, and they will clump together earlier, and thus give less time for the enzymes to degrade the amorphous matrix between the spherulites. The model presented in this paper quantifies this difference.

The simultaneous occurrence of depolymerization and crystallization typically results in a non-monotonic temperature dependence of the yield, with a maximum at an intermediate temperature [22, 32, 33]. Due to the inherent complexity of plastic waste streams, the location of this optimum cannot be anticipated a priori, emphasizing the need for a theoretical description that captures the dynamic interplay between crystallization and enzymatic depolymerization and enables prediction of reaction yields.

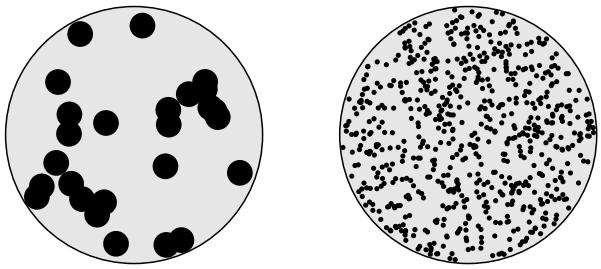

Figure 1. Sketches representing the spatial configuration of controlled preparation at two different temperatures (left: high, right: low). They serve as starting points for the degradation process. Spherulites in the right panel are chosen five times smaller and 5^3 times more numerous (in three dimensions) than in the left panel, but their volume fractions are equal.

Our approach focuses on the initial plastic morphology and explicitly accounts for thermally activated crystallization during depolymerization. The growing spherulites block enzymes' access to residual amorphous material and limit the overall yield. We present a geometric model that quantitatively describes the competition between amorphous-phase degradation and spherulite growth, providing both analytical and numerical solutions. The model tracks three key volumes over time: the spherulitic volume, the degraded amorphous matrix, and the remaining amorphous volume. Its main outputs are the ultimate fraction of polymer that will be degraded and the kinetics of this process, quantities that cannot be inferred from degradation or from crystallization alone. By combining both effects, the model provides a predictive framework for understanding and optimizing enzymatic depolymerization under recycling-relevant conditions. We illustrate its application to PET from bottles and textiles [22], demonstrating how morphological features and processing history govern reaction yield and kinetics, and suggesting experimental strategies to validate and exploit the model for process optimization.

Since the model uses only geometrical quantities, such as volumes and volume fractions, care has to be taken when comparing it with experiments. The growing spherulites are not entirely crystalline, but consist of stacked crystalline layers with amorphous polymer chains between them. The internal degree of crystallinity of a PET spherulite is typically only 30–40%. It is therefore important to distinguish between the *volume fraction filled by spherulites* (measured by light-scattering) and the *amount of crystallinity* (measured by Fourier transform infrared, FTIR, spectroscopy and by calorimetry). We account for this difference below, in section IV B, where we infer the model parameters from experimental

data.

Here we assume that the enzyme used is sufficiently thermostable so that the observed temperature dependence reflects polymer mobility and crystallization phenomena rather than enzyme inactivation. We further assume that plastic particles are suspended in an aqueous medium and saturated with enzyme, ensuring enzyme availability is not rate-limiting, and that kinetics are controlled by polymer structure.

II. A GEOMETRIC MODEL

In order to capture the main ingredients of the degradation evolution in the reaction bath, we formulate a simple Avrami-like [34, 35] geometric model for it. We take spherical geometry for both the degrading particle and the growing spherulites. The spherical geometry is not meant to literally describe spheres in the experiments, the model rather focuses on their relative overlap. We expect our results to extend also to objects that have a less well-defined boundary and different shapes. We describe the degradation of the amorphous matrix of a semi-crystalline particle by a sphere having at time t the decreasing radius

$$R_h(t) = R_{h0} + \dot{R}_h t, \quad \text{with constant } \dot{R}_h < 0. \qquad (1)$$

The radius decreasing linearly in time reflects that the volume change of amorphous matrix material is proportional to the area of surface exposed to enzymes. Embedded in the amorphous matrix we place spherulites, also modelled by spheres. The spherulites are assumed to be non-degradable; we discuss this assumption below, in section IV B. Each spherulite has a given initial radius and is growing, because at the chosen temperature the surrounding amorphous matrix tends to crystallise and is thus transformed into spherulite volume. Also here we assume a constant rate, such that a spherulite radius at time t is given by

$$R_s(t) = R_{s0} + \dot{R}_s t, \quad \text{with constant } \dot{R}_s > 0. \qquad (2)$$

We take the spherulite positions to be uniformly random distributed within the amorphous sphere, such that initially they do not stick out. Their number is denoted by N_s and the density of centers (number per volume) by N_s'.

As the radii evolve in time, the embedded spherulites come into contact and grow into each other, and the amorphous matrix is degraded from the outside, finally leaving clusters of spherulites as a remainder. The resulting geometric shapes at some intermediate time t are shown in figures 2 and 3. The characteristic egg-like shape of spherulites, with their long axis oriented towards the center of the particle, is the result of intersection of a growing and a shrinking sphere. There are three different volumes in figure 2, the spherulite volume $V_{\mathrm{sph}}(t)$ depicted in light red, the remaining amorphous volume $V_{\mathrm{am}}(t)$ in light blue, and finally in light green the volume $V_{\mathrm{deg}}(t)$ having been degraded up to time t. These three volumes always add up to the initial volume, which will serve to normalise them,

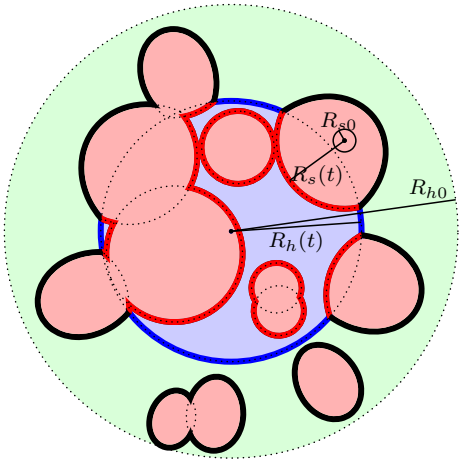

Figure 2. The three different geometric volumes used in the model, at a given time t: Degraded volume $V_{\mathrm{deg}}(t)$ (light green), amorphous volume $V_{\mathrm{am}}(t)$ (light blue) and spherulite volume $V_{\mathrm{sph}}(t)$ (light red). The thick solid curves show the interfaces between these volumes.

$$V_{\mathrm{am}}(t) + V_{\mathrm{sph}}(t) + V_{\mathrm{deg}}(t) = \frac{4\pi}{3} R_{h0}^3 =: V_{\mathrm{tot}}. \qquad (3)$$

Figure 2 shows also the interfaces between the different volumes. The rate at which amorphous volume is converted into spherulite volume is proportional to the area of the amorphous–spherulite interface $S_{\mathrm{am,sph}}$ (dark red in figure 2),

$$\frac{d}{dt} V_{\mathrm{sph}}(t) = \dot{R}_s \, S_{\mathrm{am,sph}}(t). \qquad (4)$$

This quantity is (up to a constant scaling factor corresponding to the internal degree of crystallinity of the spherulites) accessible by calorimetry experiments, by light-scattering or by Fourier transform infrared (FTIR) spectroscopy [22, 36, 37]*. We model the spherulites to be inert to enzymes: Their part sticking out of the amorphous matrix (thick black curves in figure 2) does not change shape anymore, and the spherulites grow only inside the amorphous sphere. At the same time they block access of enzymes to the amorphous matrix and thus effectively reduce the degradation rate. The degradation

* To be more precise, light-scattering measures the *volume fraction of spherulites*, whereas Fourier transform infrared (FTIR) spectroscopy measures the total *degree of crystallinity*. The scaling factor is constant in the temperature range used here. We thank our reviewer for stressing this point, and we fully account for the difference between these two quantities below, in section IV B.

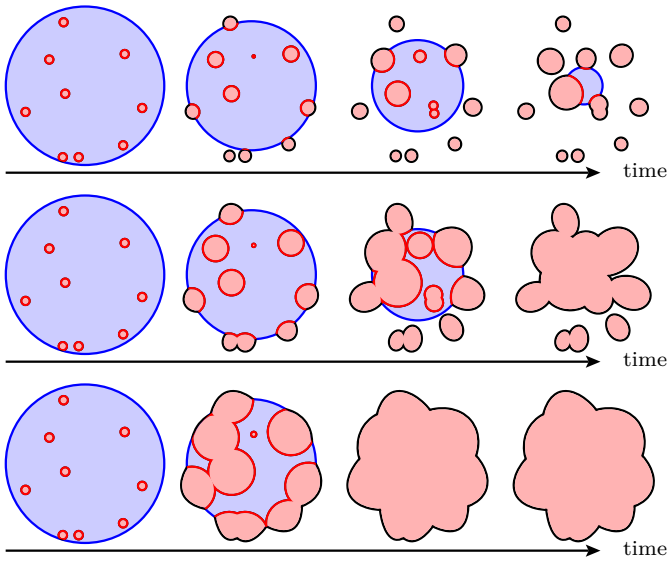

Figure 3. Evolution in time of the geometry used in the model: The amorphous volume (blue) is degraded, the spherulites (red) grow (and possibly nucleate) only within the amorphous phase, finally remaining as connected clusters of egg-shaped objects (black curves). The three rows correspond to different growth rates of spherulites with the same degradation rate of the amorphous phase.

of the amorphous volume is thus proportional to the area of the exposed amorphous–solute interface $S_{\mathrm{am,deg}}$ (thick dark blue curves in figure 2),

$$\frac{d}{dt}V_{\mathrm{deg}}(t) = |\dot{R}_h| S_{\mathrm{am,deg}}(t). \tag{5}$$

Equations (1)–(5) are a system of ordinary differential equations (ODE) for the three time-dependent volumes. Before solving them let us look at two special cases where they are decoupled.

We denote units of length and time by $\mathcal{L}$ and $\mathcal{T}$, respectively.†

A. Degradation alone

In the absence of spherulites, there is only degradation of the wholly amorphous particle, and the relative volume of the amorphous matrix is simply

$$\frac{V_{\mathrm{am}}(t)}{V_{\mathrm{tot}}} = \left(\frac{R_h(t)}{R_{h0}}\right)^3, \tag{6}$$

† In the parameters of figures 4, 5, and 6 we do not fix values for units of length and time yet. We focus on the difference of timescales, not on their absolute value. We will fix the units when comparing experimental and simulation data, in section IV.

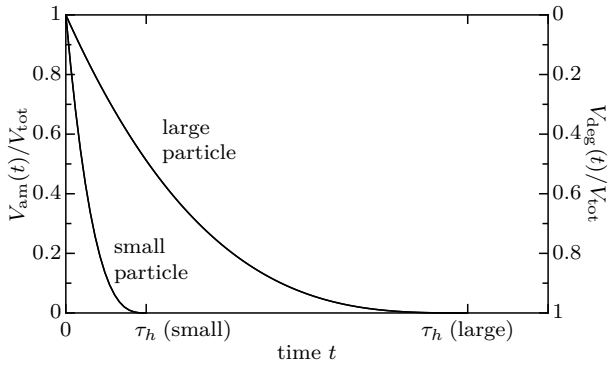

parameters:†	R_{h0}	$\dot{R}_h$	τ_h
small particle	$\mathcal{L}$	$-\mathcal{L}/\mathcal{T}$	$\mathcal{T}$
big particle	$5\mathcal{L}$	$-\mathcal{L}/\mathcal{T}$	$5\mathcal{T}$

Figure 4. Evolution in time of relative amorphous and of so-far degraded volume, without spherulites, according to equations (3) and (6). The timescale of degradation, τ_h is defined in equation (7).

with the time-dependent radius given by equation (1). Small particles are degraded more quickly, even for the same enzyme activity, because they expose more surface relative to their volume. This effect can be seen in figure 4.

The timescale of degradation is the time on which a purely amorphous particle vanishes, see equation (1). We define it as

$$\tau_h := \frac{R_{h0}}{|\dot{R}_h|}. \tag{7}$$

B. Spherulite growth alone

The central ingredient of the model places it in the class of *Avrami* models (sometimes also linked to the name of Kolmogorov and others) [35]. These models capture the mutual overlap of spheres, placed randomly in unbounded space at a density N_s' of centers per volume. In the limit of many spheres, the common volume of the spheres is found to be an exponential function of the sum of individual volumes. The volume fraction $V_{\mathrm{sph}}(t)/V_{\mathrm{tot}}$ thus starts at an initial (small) value, then increases, and finally converges to unity, when all space is filled with spherulites. The formula of it reads

$$\frac{V_{\mathrm{sph}}(t)}{V_{\mathrm{tot}}} = 1 - \exp\Big(-N_s' \tfrac{4\pi}{3} R_s^3(t)\Big). \tag{8}$$

This function is plotted in figure 5 for the two densities of figure 1 (but without boundary and therefore no degradation). The two different initial states, although having the same volume fraction and the same growth parameter $\dot{R}_s$, converge at very different timescales.

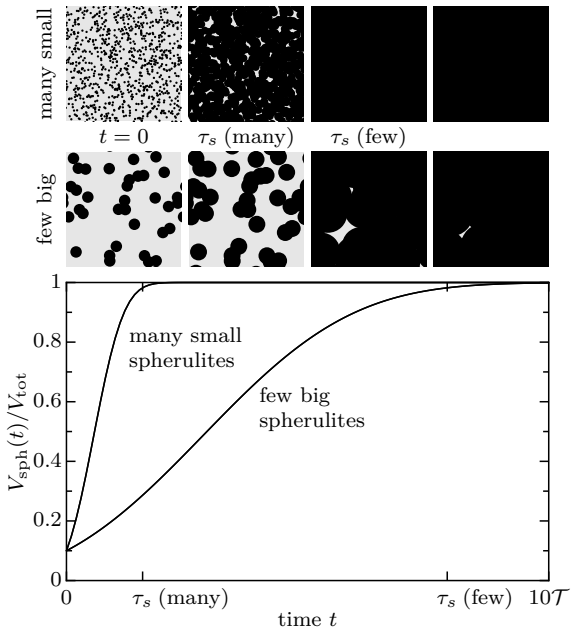

parameters:†	R_{s0}	$\dot{R}_s$	N'_s	τ_s
many small	$0.02\mathcal{L}$	$0.03\mathcal{L}/\mathcal{T}$	$3144.12/\mathcal{L}^3$	$1.6\mathcal{T}$
few big	$0.10\mathcal{L}$	$0.03\mathcal{L}/\mathcal{T}$	$25.15/\mathcal{L}^3$	$7.9\mathcal{T}$

Figure 5. Evolution in time of relative spherulite volume in bulk, according to equation (8). The timescale of spherulite growth, τ_s is defined in equation (9). Top panels: spatial sketches at chosen times.

In order to identify the relevant timescale for spherulite growth, let us first look at a rather dilute case, where spherulites are mostly well separated initially ($N'_s \ll 1$), at the time when particles were put into the reaction bath. They all start with the same radius R_{s0} and grow at the same rate $\dot{R}_s$. After a typical time τ_s the spherulites are not well separated anymore but start to grow into each other. It is

$$\tau_s := \frac{1}{\dot{R}_s}\left(\frac{1.28}{\sqrt[3]{N'_s}} - 2R_{s0}\right). \tag{9}$$

The quantity in parentheses is referred to as the *ligament thickness* in the context of toughening of polymers [38, 39]. For the same initial spherulite volume fraction $V_{\rm sph}(0)/V_{\rm tot} \approx N'_s \frac{4\pi}{3} R_{s0}^3$ we can have different timescales τ_s, as explained above. For the examples in figure 1 we expect a ratio of five of their respective values. If there were no degradation, we would obtain the filling curves in figure 5.

When we look at spherulites not in unbounded space but inside the degrading particle, the Avrami approach leading to equation (8) becomes inapplicable for two reasons: First, the spherulite volume inserted into the exponential function in equation (8) is to be corrected when it is only partly inside the particle. Second, and more importantly, there is a subtle implicit assumption underlying equation (8), namely that the spherulites have to be uniformly distributed in space. The boundary of the particle breaks this uniformity, and a spherulite close to it will not be isotropically surrounded by other spherulites. As a result, the function (8) does not hold.

C. Coupled growth and degradation

In the general case, when spherulites grow within the eroding particle, the growth curves in figure 5 are limited by the decreasing curves in figure 4 because spherulites cannot grow outside the amorphous matrix. At the same time also the degradation of amorphous matrix is reduced because the spherulites block the access of enzymes to it.

The model equations (1)–(5) express this mutual influence of spherulites and degradation. They result in three volumes as functions of time, namely in spherulite volume $V_{\rm sph}(t)$, in so-far degraded amorphous volume $V_{\rm deg}(t)$, and in remaining amorphous volume $V_{\rm am}(t)$. The combined dynamics leads to a coupled pair of curves, one for growth, one for degradation. The two curves join each other at the end of the process when $V_{\rm am}(t)$ vanishes. Figure 6 shows these curves for four different cases. The three volumes $V_{\rm sph}(t)$, $V_{\rm am}(t)$, and $V_{\rm deg}(t)$ are the vertical distances between curves and coordinates axes, respectively. Since the three volumes add up to the initial total volume $V_{\rm tot}$, plotting them together in one graph seems the natural way to present the solution, and it allows also to see their relation at once. At early times, the curves in figure 6 resemble those in figures 4 and 5, but then growth and degradation mutually influence each other.

Due to the degradation, the final spherulite volume is not the total volume, but some fraction of it. Its terminal value tells us what portion of the amorphous matrix has been degraded and what portion crystallised. This fraction and the typical time when it is reached are the main quantities of interest, in particular how they depend on the parameters $\dot{R}_h$, $\dot{R}_s$, R_{h0}, R_{s0}, and N'_s. In reality, these model parameters depend themselves on the materials used, on the temperature, and on the way the sample was prepared.

The top panel of figure 6 shows the influence of whether the initial crystalline volume is split into many small spherulites or few big ones. We thus come back to the initial question raised around figure 1: Is the overall initial crystallinity sufficient to predict the outcome of the degradation process or are there other important parameters to consider? Here, the corresponding model parameters N'_s and R_{s0} play an additional, decisive role. In this simulation we constrain the initial crystallinity to the same value, but when the same initial volume is split into many small spherulites, less material is finally degraded. From the different pairs N'_s, R_{s0} we obtain two different timescales τ_s which compare differently with the given timescale τ_h.

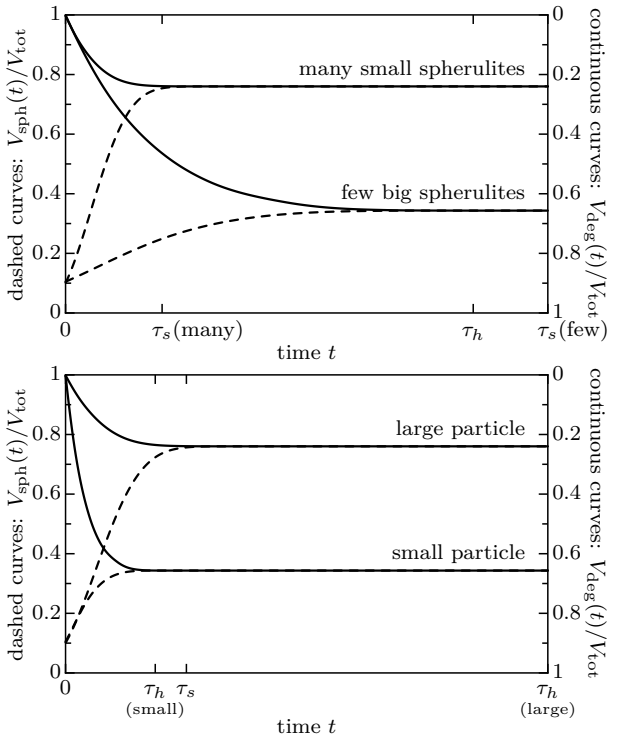

parameters:†	R_{s0}	$\dot{R}_s$	N'_s	R_{h0}	$\dot{R}_h$
many small spherul.	$0.02\mathcal{L}$	$0.2\mathcal{L}/\mathcal{T}$	$3145.0/\mathcal{L}^3$	$\mathcal{L}$	$-\mathcal{L}/\mathcal{T}$
few big spherulites	$0.10\mathcal{L}$	$0.2\mathcal{L}/\mathcal{T}$	$25.2/\mathcal{L}^3$	$\mathcal{L}$	$-\mathcal{L}/\mathcal{T}$
large particle	$0.10\mathcal{L}$	$0.2\mathcal{L}/\mathcal{T}$	$25.2/\mathcal{L}^3$	$5\mathcal{L}$	$-\mathcal{L}/\mathcal{T}$
small particle	$0.10\mathcal{L}$	$0.2\mathcal{L}/\mathcal{T}$	$25.2/\mathcal{L}^3$	$\mathcal{L}$	$-\mathcal{L}/\mathcal{T}$

Figure 6. Numerical solution of the model: evolution in time of the three volumes $V_{\rm sph}(t)$, $V_{\rm deg}(t)$, and $V_{\rm am}(t)$. Upper panel: for the same τ_h and different τ_s, shown are the two cases of figure 1; τ_s is varied by varying N'_s, R_{s0}, while keeping the initial volume constant. Lower panel: for the same τ_s and different τ_h, by varying R_{h0}. All volumes are normalised by $V_{\rm tot}$. $V_{\rm sph}/V_{\rm tot}$ is drawn as dashed curves, with values referring to the left axis, while $V_{\rm deg}/V_{\rm tot}$ is drawn as continuous curves referring to the right axis. $V_{\rm am}/V_{\rm tot}$ is the vertical distance between the pairs of curves, according to equation (3).

The lower panel of figure 6 shows the effect of different timescales τ_h, as compared to a single τ_s. This corresponds for example to different sizes R_{h0} of particles, obtained from finer/coarser milling. As expected, small particles are degraded more efficiently, both in final yield, and in timescale.

In the model we did not specify units of space and time yet. The curves do not actually depend on the five parameters given, but only on three dimensionless ones. One choice for the set of dimensionless parameters would be $\dot{R}_s/\dot{R}_h$, R_{s0}/R_{h0}, and $N'_s R_{0s}^3$. The same curves can be obtained also from different sets of parameters: For example, a bigger particle can be compensated by bigger spherulites, which have to be less numerous in order to keep the volume fraction unchanged. We will fix units of length and time in section IV when extracting model parameters from experimental data.

III. NUMERICAL ALGORITHM

Our approach to obtain volumes as a function of time is to take a randomly chosen initial geometric configuration, that is a fixed finite set of sphere centers and initial radii, and discretise the evolution equations (1), (2) for the radii. We present in this section a new numerical algorithm devised to efficiently obtain at each time-step all the required geometric volumes, surface areas, and curve lengths. In particular, the surface areas on the right-hand sides of equations (4) and (5) are necessary.

A. Double tessellations of space

The main task of the numerical algorithm is to take into account the overlaps of spherulites without counting them twice or more. We use a Voronoi tessellation [40] of space for this, in which every Voronoi cell corresponds to one sphere. The Voronoi tessellation must be adapted to the positions and to the radii of the spheres. Our implementation makes use of the numerical framework CGAL [41, 42] because it allows to treat *weighted* Delaunay/Voronoi tessellations of spheres which all have different radii (sometimes also referred to as *regular* tessellation); this reflects the possibility that spherulites can vary in their initial radius, or even nucleate at later times.

The weighted tessellation captures all the mutual intersections between growing spherulites. The usual weighted tessellation, however, only considers spheres being outside each other, it does not provide the intersections of the amorphous sphere with the spherulite spheres inside. We present here a new algorithm, which is an extension of the usual weighted triangulation. Geometrically, the situation can be seen as a "double" oriented and weighted tessellation, where the Voronoi cells of spherulites are all *contained in* the Voronoi cell of the amorphous one. This situation is depicted in the right column of figure 7.

The middle row of figure 7 visualises the construction of how a Delaunay/Voronoi pair of tessellations can be translated into a lower-convex-hull problem in a space that has one additional "lifted" coordinate [43, 44]. The visualisation is limited to a single spatial dimension, plus the lifted one; this one-dimensional tessellation is shown in the lowest row of figure 7. The extension to two and three spatial dimensions requires geometric abstraction in the reader's imagination: for the numerical results in this paper we always used three spatial dimensions. The left column of figure 7 depicts a simple Delaunay/Voronoi pair of tessellations: The spatial coordinates (x, y) of each point are lifted to a paraboloid, turn-

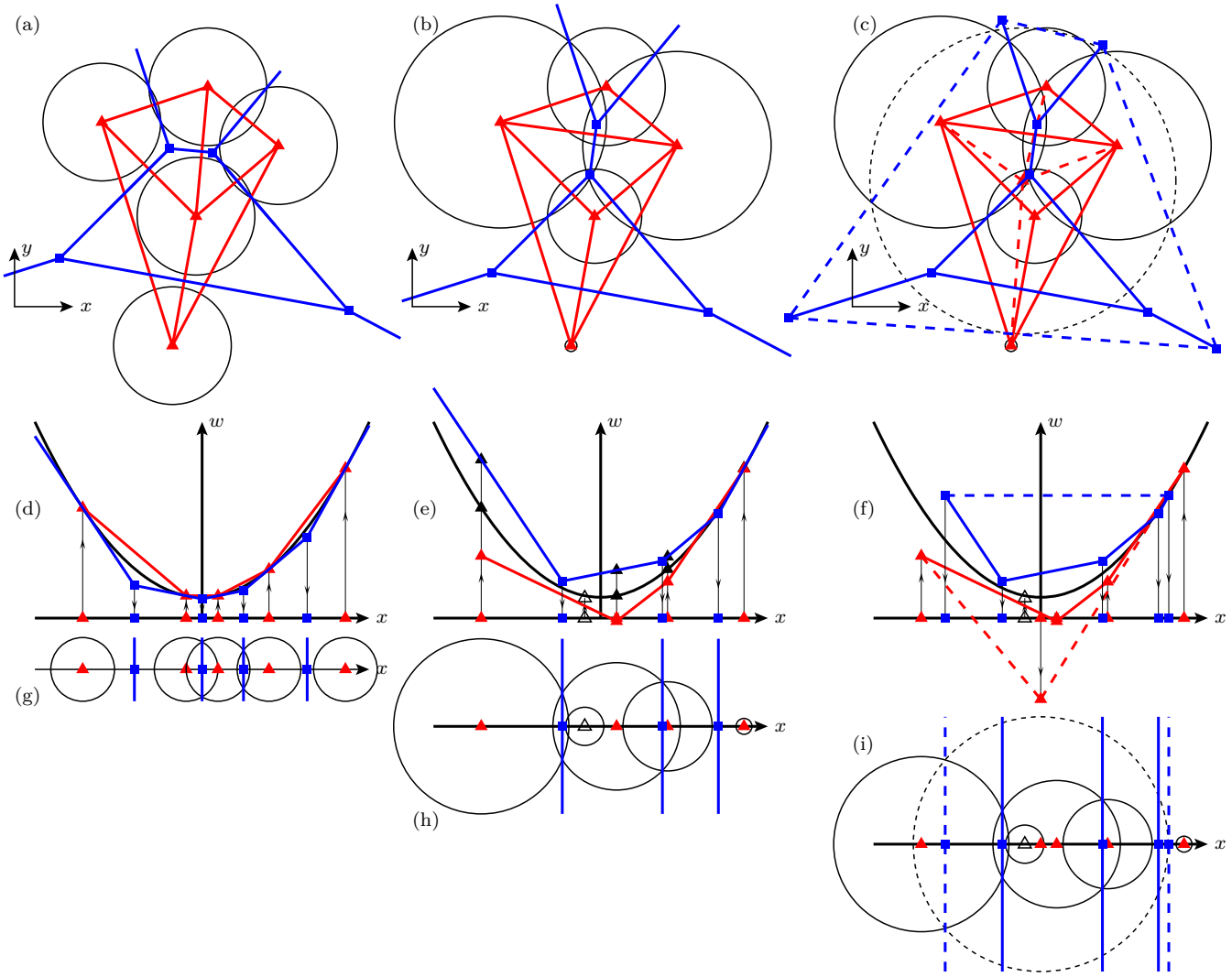

Figure 7. Visualisation of three types of Delaunay/Voronoi tessellation pairs. The input spheres are shown as black circles, Delaunay tessellations are drawn in red, with little triangles at vertices, and Voronoi tessellations are drawn in blue, with little squares at vertices. Input spheres that are not part of the Delaunay tessellation have open triangles at their center. The left column shows ordinary Delaunay/Voronoi, where all spheres have the same radius; the middle column is a *weighted* Delaunay/Voronoi tessellation with differently sized spheres; and the right column shows a *double* oriented and weighted tessellation with the dashed sphere having the others on its inside instead of the outside. The Voronoi cell corresponding to the dashed sphere is also drawn with dashed lines. The top row gives some examples of two-dimensional tessellations. The middle row visualises how Delaunay/Voronoi tessellations can be constructed using coordinates lifted to a paraboloid and vertically shifted according to the weight of the points (lines with upwards pointing arrows). The Voronoi vertices result from a lower convex plane construction in lifted space (downwards pointing arrows). The method works in any spatial dimension, but visualisation is here limited to one spatial dimension, that is why we show the one-dimensional tessellation corresponding to the paraboloid construction in the bottom row.

ing into $(x, y, x^2 + y^2)$. The lower convex hull (depicted in red) of these points defines which point is a Delaunay vertex, and which ones are neighbors. Bringing this hull down to the (x, y) coordinates defines the Delaunay cells. In each lifted point we construct a tangent plane to the paraboloid (depicted in blue), which intersect and together form another convex hull. Bringing this second hull down to the (x, y) coordinates defines the Voronoi vertices and cells.

The middle column of figure 7 shows the effect of different radii on the construction. We lower the lifted coordinate of input spheres by their squared radius, also called "weight", to $(x, y, x^2+y^2-r^2)$, and take again the lower convex hull to find the Delaunay cells. The weights have influence on who is neighbor to whom, and it can even happen that a sphere does not contribute to the tessellation at all, because it is too small and too close to a bigger one (see the open triangles in panels e,h). The

tangent planes to the paraboloid are lifted by the sphere weights, thus passing through $(x, y, x^2+y^2+r^2)$. Again, their intersections define the Voronoi tessellation. Observe that the lifted planes' intersections coincide with the intersection lines of spatial circles.

The right column of figure 7 shows the addition of the amorphous sphere (dashed). This is the situation we have to address. Our algorithm consists in combining two tessellations, one from the spherulites only, and one into which we insert also the amorphous sphere. We can intersect the two tessellations only if they have some outermost vertices in common: If necessary, we surround the whole ensemble with zero-weight dummy points such that there are always common outermost Delaunay vertices. The two tessellations form a closed body in lifted coordinates, as is visible in panel (f) of the figure. The same is true of the body formed by vertically shifted tangent planes. Both bodies appear as two overlaying tessellations when projected down from lifted coordinates to space, see panels (i) and (c). As a result, there is a Voronoi cell dual to the shrinking amorphous sphere (blue dashed), which is partitioned into Voronoi cells, each dual to one growing spherulite. This double tessellation allows to measure surface areas of spherulites embedded into the amorphous matrix, and also the lengths of triple-lines of growing spherulites, shrinking amorphous particle, and the outer void.

B. Geometric measures

At every time step, we measure several geometric quantities, namely the volume of embedded spheres, the area of the amorphous–solute interface, the area of the amorphous–spherulite interface, and the arc lengths of the amorphous–spherulite–solute interlines. This is achieved by cutting each Voronoi cell into wedge-shaped simplices, making use of the right angles between Delaunay edges and Voronoi faces, and between Delaunay faces and Voronoi edges. In such an orthogonal simplex the contained spherical volume, spherical surface, and circular arcs are known analytically [42, 45, 46]. We add up these contributions from every simplex of every Voronoi cell of the tessellation. In the sum, each contribution carries a sign which depends on how the Voronoi face cuts the Delaunay edge, on how the Delaunay face cuts the Voronoi edge, and on whether the Voronoi cell corresponds to the amorphous particle or not.

During the time-stepping, the arc lengths of amorphous–spherulite–solute interlines are integrated to yield the surface area sticking out of the particle (black in figure 2), the amorphous–spherulite interface area is integrated to give the spherulite volume, and the area of the amorphous–solute interface is integrated to give the degraded volume.

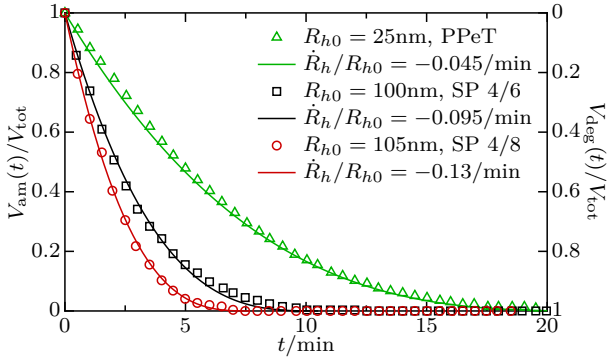

Figure 8. Degradation of purely amorphous nanoparticles. Experimental data taken from Welzel's thesis [16, Fig. 5-10]. PPeT is polypentylene terephthalate, consisting of 1,5-pentanediol and terephthalic acid. SP 4/6 is a saturated polyester consisting of 1,4-butanediol and adipic acid. SP 4/8 is a saturated polyester consisting of 1,4-butanediol and suberic acid.

IV. FINDING MODEL PARAMETERS FROM EXPERIMENTS

The most noble aim of any model is to be predictive in the sense that it can guide experiments. Here, for given experimental parameters the model provides the final degradation percentage and the timescale. Reversely, if used as a fitting method, it can provide the model parameters for given experimental degradation/growth curves. Our plan for this section is to obtain the degradation parameters R_{h0}, $\dot{R}_h$ from data without spherulite growth, and to obtain the spherulites parameters N_s', R_{s0}, $\dot{R}_s$ from growth experiments without degradation. The experimental procedure and materials are described in reference 22.

A. Degradation parameters

In most cases degradation and growth occur together, which is the whole point of the model. There is one exception, though. Welzel [16] observed that if the plastic particles are small enough, up to 200 nm, they are totally amorphous. Her two main arguments are that the degradation rates do not depend on preparation temperatures, and that the cleaving energies are the same as for liquid polymers [16, p. 77]. For these nanoparticles she measured the degradation, and we show her data in figure 8. For this degradation, Welzel proposed and confirmed the same degradation evolution as we do in equation (1), where the radius decreases linearly in time. Data and model match very well.

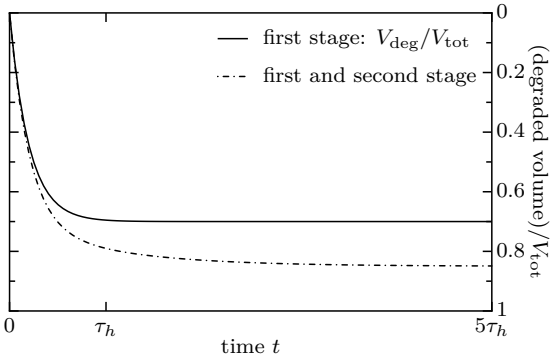

Figure 9. Schematic sketch of the degradation process happening in two stages: First the degradation of main amorphous matrix, then the degradation of amorphous material in the spherulites which grew in the first stage and were released into the solute. These curves do not come from numerical modeling but are illustrative sketches.

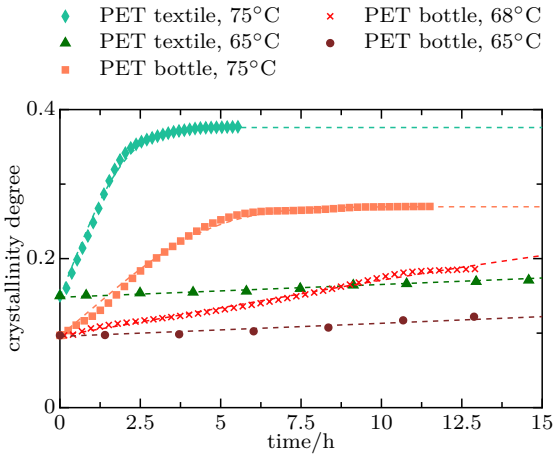

Figure 10. Symbols: Experimental isothermal calorimetry data for crystallinity growth in PET particles, in buffer, without degradation. The particles are two different plastic waste types, from bottles or from textiles, and are crystallised at different temperatures [22]. Dashed curves: Fits according to equation (10), resulting in the optimal parameters given in table (11).

B. Non-crystalline material in spherulites

A major simplification done in the model concerns the definition of spherulite material. In the model any point in space is either in a spherulite, or in the amorphous matrix, or degraded, and all material in the spherulites is effectively taken as "crystalline". In experiments this is not absolutely true [17, page 176]. When we measure the degree of crystallinity by isothermal calorimetry, together with a DSC scan at the end [22], then even in samples in which spherulites have grown to cover all space, we do not measure a degree of crystallinity of 100%, but rather 30%. This is caused by internal structure of the spherulites which comprises constrained amorphous polymer segments [47, 48] as loops and chains joining crystalline lamellae. The DSC experimental method measures only the fusible, crystalline part of their filling but not the amorphous part.

In order to overcome this discrepancy, we need to rescale the measured crystallinity to arrive at the spherulite volume. We take the spherulites to be crystalline to a certain percentage, which does not change with temperature, and which is constant in time. It can therefore be read off from the terminal plateau values at 75°C in figure 10, where we can assume that all space is covered by spherulites. For example, the PET bottles treated at 75°C go up to a terminal crystallinity degree of $A = 27\%$. At the end, all volume is filled by spherulites, thus $V_{\rm sph}/V_{\rm tot} = 1$. For those data lines in figure 10 which do not reach the plateau level in the observation time, we assume the same final level as their counterparts at higher temperatures: It is the same material and underwent the same preparation. These values are marked with a symbol (‡) in tables (11) and (12).

Another consequence of the partial order within spherulites is they are not completely inert to enzymes but will be degraded as well, however on a longer timescale. Welzel [16] found a timescale at least five times longer than for the amorphous matrix. We understand the degradation as a two-stage process in which first the amorphous matrix is degraded and spherulite clusters are released, and second the spherulite clusters are degraded as well. Figure 9 visualises the concept. The second stage means that in experiments we will not see a well-defined final degradation level, but that the values continue to change slowly. This can be seen below, in figure 12.

C. Spherulite parameters

Figure 10 shows the experimental curves of growing crystallinity in PET particles obtained from bottles and textiles. The initial particle radius is around $R_{h0} = 80\mu$m. A fit with an Avrami function needs three parameters,

$$\chi(t) = A\Big[1 - \exp\Big(-\frac{4\pi}{3}(B + Ct)^3\Big)\Big], \qquad (10)$$

with the optimal values[‡]

fit of function (10):	A	B	C
PET textile, 75°C	0.37	0.49	1.5×10^{-1}/h
PET textile, 65°C	0.37[‡]	0.49[‡]	2.5×10^{-3}/h
PET bottle, 75°C	0.27	0.47	7.2×10^{-1}/h
PET bottle, 68°C	0.27[‡]	0.47[‡]	1.5×10^{-2}/h
PET bottle, 65°C	0.27[‡]	0.47[‡]	3.5×10^{-3}/h.

(11)

[‡] Values marked with a symbol (‡) are imposed instead of resulting from a parameter fit.

In the data time-series, the final level of crystallinity is visible only for the highest temperature, namely 75°C; the parameter A is then part of the fitting procedure. For lower temperatures, the final level is not included in the data, but we assume that it does not depend on the processing temperature, only on preparation, therefore we impose it in the fitting procedure. The same applies to the parameter B, which reflects the initial size of spherulites. In table (11) and in the following tables, imposed values are marked with a symbol (‡).

In order to obtain the model parameters from these fits, we further need a value for N_s'. Jabarin's publication [49] about the haze in dried PET sheets without initial crystallinity gives a distance between nucleation sites of roughly 4μm, for temperatures of 115°C to 130°C, see Fig. 6 there. Lacking more precise information, we use this value for N_s' for the PET particles.

The correspondence to model parameters is $B = (N_s')^{1/3} R_{s0}$, $C = (N_s')^{1/3} \dot{R}_s$, and A translates into V_{tot} with a suitable factor which will not be used. Together with the fit values of table (11) we now obtain the following model parameters for spherulites:

	$(N_s')^{1/3}$	R_{s0}	$\dot{R}_s$
PET textile, 75°C	0.31/(μm)‡	1.6μm	$4.9\times10^{-1}\mu$m/h
PET textile, 65°C	0.31/(μm)‡	1.6μm‡	$7.9\times10^{-3}\mu$m/h
PET bottle, 75°C	0.31/(μm)‡	1.5μm	$2.3\times10^{-1}\mu$m/h
PET bottle, 68°C	0.31/(μm)‡	1.5μm‡	$4.8\times10^{-2}\mu$m/h
PET bottle, 65°C	0.31/(μm)‡	1.5μm‡	$1.1\times10^{-2}\mu$m/h.

(12)

D. Depolymerisation hindered by spherulites

The experimental depolymerisation yield from PET particles is shown in figure 11, from the same materials and at the same temperatures as figure 10. The depolymerisation was done using the enzyme hydrolase LCC-ICCG [1, 22]. The model's parameter $\dot{R}_h$ accounting for depolymerisation is encoded in the initial slope of the curves in figure 11. If the initial crystallinity is negligible, then the initial slope of the depolymerisation curves is simply given by the parameter combination $\dot{R}_h/R_{h0}$, see figure 4 for an example.

If, however, a considerable part of the amorphous–solute interface is covered by spherulites, they block the enzymes' access to amorphous material. Only a fraction $\exp\left(-\frac{4\pi}{3} N_s' R_{s0}^3\right)$ of the shrinking sphere's surface is exposed to enzymes, and the degradation is reduced by the same factor. The factor has the same exponential form as seen in equation (8), which is characteristic of an Avrami argument. Indeed, it has the same origin, only that here we do not have spheres overlapping in space, but circles overlapping on the particle's surface. The value of the factor can be calculated from the values

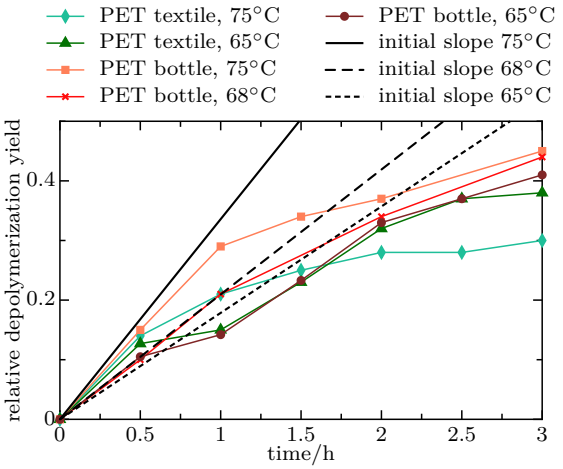

Figure 11. Symbols: Experimental data from depolymerisation of PET particles, in buffer [22]. Fits of function (13) to the initial part of the curves result in the optimal parameters given in table (14). Their initial slopes, as given in table (15) are visualised by the black lines.

given in table (12), and the initial slope of the curves can be obtained from figure 11. To obtain these slopes, we first fit a smooth function locally to the data at short times, namely the following cubic function,

$$D\Big[1-(1-Et)^3\Big]. \tag{13}$$

The fit yields the optimal parameters D and E,

fit of function (13):	D	E	$3DE$
PET textile, 75°C	0.31	0.34/h	0.31/h
PET textile, 65°C	0.64	0.096/h	0.18/h
PET bottle, 75°C	0.42	0.29/h	0.36/h
PET bottle, 68°C	0.68	0.1/h	0.21/h
PET bottle, 65°C	0.86	0.067/h	0.17/h

(14)

The slope at time zero is then given by $3DE$, which equals $(-3\dot{R}_h/R_{h0})\exp(-\frac{4\pi}{3} N_s' R_{s0}^3)$ in terms of the model parameters. The fitting procedure was carried out individually for every experimental curve. However, the enzyme activity is expected to depend only on the temperature, and not on the material or the preparation. Indeed, the fitting nicely groups the initial slopes by their processing temperature. We can thus average for each temperature,

average initial slope:	$\langle 3DE\rangle$
75°C	0.34/h
68°C	0.21/h
65°C	0.18/h.

(15)

Together with the radius R_{h0} of the particles, which we take to be 80μm, we obtain the model parameters for

depolymerisation,

	R_{h0}	$\dot{R}_h$
PET textile, 75°C	$80\mu\text{m}^\ddagger$	-13.7μm/h
PET textile, 65°C	$80\mu\text{m}^\ddagger$	-8.1μm/h
PET bottle, 75°C	$80\mu\text{m}^\ddagger$	-15.0μm/h
PET bottle, 68°C	$80\mu\text{m}^\ddagger$	-8.7μm/h
PET bottle, 65°C	$80\mu\text{m}^\ddagger$	-7.2μm/h.

(16)

V. RESULTS AND DISCUSSION

In the above section we learned how to get the model parameters for depolymerisation and for spherulite growth from experimental data. With the values in table (16) we obtained the parameters R_{h0}, $\dot{R}_h$ characterising degradation, and with the values in table (12) those characterising spherulites, N_s', R_{s0}, $\dot{R}_s$. Now we can use both sets of parameters in our model to make a numerical prediction for combined degradation and spherulite growth. Figure 12 shows this prediction for the depolymerisation of PET particles from the two different sources of waste and different temperatures and compares it with the experimental data.

For PET from textile waste, the model fits the experimental data very nicely, see the upper panel of figure 12. Both the final yield and the timescale are predicted by the model, at both temperatures. The match between model and data is a real success of the model and of all its underlying assumptions. We reiterate here that the Avrami model describes overlap of spheres with well-defined sharp boundary, which works for spherulites in textile PET waste, and that in the model the final level of depolymerisation is only indirectly given by the final level of crystallisation. Also here the assumption of sharply bounded spherulites enters. This final level has been accessible from experiments only for 75°C, see figure 10. At 65°C we had to deduce it from the 75°C data. And finally, the rate of depolymerisation has been estimated from the very first part of the depolymerisation data only. Altogether, the spectacular matching of model prediction and experimental data in the upper figure 12 corroborates the chain of arguments and approximations we used in the course of sections II and IV.

The model slightly underestimates the depolymerisation of PET textile for times later than eight hours. Especially the data at 65°C seem to increase slowly again after having levelled before. We attribute this slow increase to the second-stage depolymerisation described in section IV B.

For PET from bottle waste, the comparison of model and experiment is shown in the lower panel of figure 12. Here, the model matches experimental data up to five hours of depolymerisation. After that, there are substantial deviations. We think that they have two reasons, first

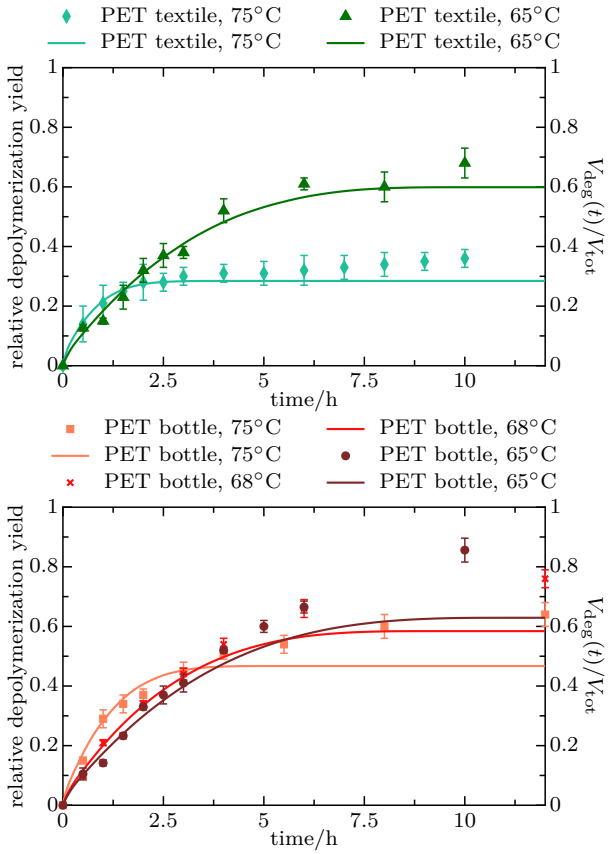

Figure 12. Comparison of the numeric model (curves) with experimental depolymerisation data (symbols). The symbols refer to the left axis, while the curves refer to the right axis. Model parameters are given in tables (12) and (16).

that the growing spherulites do not have a well-defined boundary and the model idea of overlapping spheres is thus too simplistic. Second, that these spherulites have a highly amorphous content, and the second-stage depolymerisation sets in early and is quite pronounced. We remind the reader of figure 10 where the highest observed crystallinity degree in PET bottles is only around 27%.

We like to draw the reader's attention to an interesting feature of figure 12: The degradation curves at high temperature start at a steeper initial slope than those at low temperature, one would expect also a higher terminal yield. The observed terminal yields, however, are actually lower—the curves reverse their order. The explanation for this is the spherulite growth, which reduces the effective degradation, and which is more effective at higher temperatures. The results in figure 12 show that this effect is strong enough to revert the first intuition from initial degradation slopes. It is thus useful to show the degradation and the growth curves together, in the same fashion as we did already in figure 6. This is done in figure 13.

The two timescales τ_s, τ_h, defined in equations (9), (7), provide a useful estimate to describe the curves in fig-

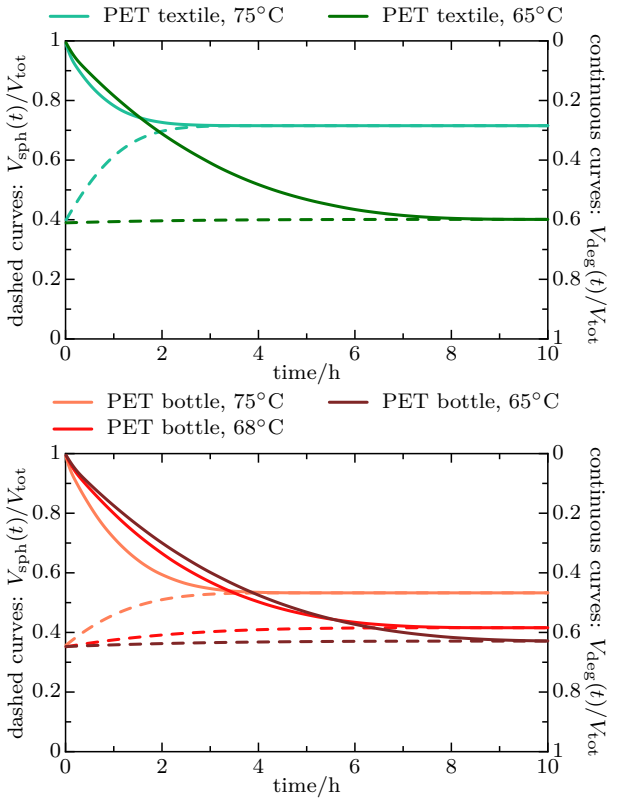

Figure 13. Numerical solution of the model, applied to PET particles: combined dynamics of amorphous degradation and spherulite growth. Model parameters are given in tables (12) and (16). The degradation curves are the same as in figure 12.

ure 13. From tables (12) and (16) we obtain the following values,

	τ_s	τ_h
PET textile, 75°C	1.9h	5.8h
PET textile, 65°C	120h	9.9h
PET bottle, 75°C	4.6h	5.3h
PET bottle, 68°C	23h	9.2h
PET bottle, 65°C	95h	11.1h.

(17)

When $\tau_s \gg \tau_h$ then spherulite growth is sufficiently slow that nearly all initially amorphous material will be degraded. The curves at 65°C in figure 13 are this case. At 75°C there is no clear separation of timescales, and degradation and growth both contribute to the final outcome. This has been clearly visible in figure 6, and we show it again in figure 13 for the parameters from the PET degradation experiments.

A. Varying the initial crystallinity

In this section we vary the parameters of tables (12) and (16) to make predictions for the depolymerisation

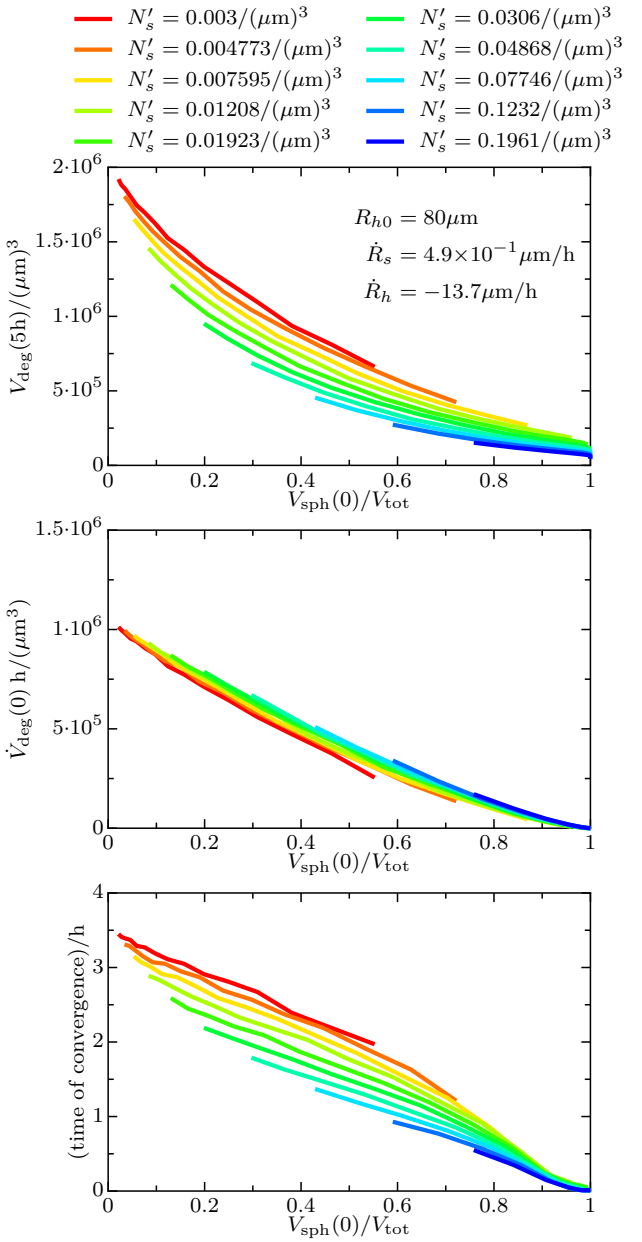

Figure 14. The effect of initial morphology and of initial spherulite volume: Numerical solution of the model, applied to PET particles from textiles, treated at 75°C. Shown are three chosen quantifiers for the yield of monomers, as a function of two parameters R_{s0} and N_s'. All other parameters are constant as given in tables (12) and (16). R_{s0} and N_s' are related to the initial filling by spherulites $V_{\rm sph}(0)/V_{\rm tot}$ via equation (8).

yield. We vary those parameters for which we did not do experiments. It is common practice to characterise the output of enzymatic degradation by key quantifiers, such as the yield of monomers after a fixed amount of time, or the initial yield rate [50]. These quantifiers are simpler than the full degradation curve. Figure 14 shows predictions from the numerical model for three such quantifiers:

for the amount of degraded monomers after five hours (top panel), for the initial slope of the degradation curve (middle panel), and for how long the degradation process takes (bottom panel). For the latter convergence time we take the time when the growth and degradation curves, such as shown in figure 13, approach each other closer than 5% for the first time. We base the model parameters for figure 14 on those for PET textile at 75°C, as given in tables (12) and (16) and then vary both N_s' and R_{s0}, independently. These two parameters determine the initial filling by spherulites $V_{\rm sph}(0)/V_{\rm tot}$ by equation (8).

In the top panel of figure 14 we find again the same message as in figure 6: Many small spherulites lead to lower degradation yield than few big spherulites. Notice that for a given $V_{\rm sph}(0)/V_{\rm tot}$, increasing R_{s0} means decreasing N_s', and vice-versa. In the bottom panel of figure 14 we see that many small spherulites reach the final levels earlier than few big spherulites. We found the same message from the conceptual parameters in figure 6.

The middle panel of figure 14 quantifies the initial rate of degradation as a function of the parameters N_s' and R_{s0}. The spread of these values is much less than in the top panel of the figure. Moreover, the order of the curves is inverted, that is more and smaller spherulites lead to a smaller initial slope, despite an increased yield after five hours. The same inversion is visible in figure 12. For the materials we used, the initial rate of degradation is thus no indicator for the final yield of degradation.

B. Varying the particle size

Figure 15 shows again the three quantifiers, now varying the particle size R_{h0}. This is an important parameter for practical application, because it reflects how finely the plastic waste has been milled. In the top panel of figure 15 we see a crossover of yield from volume-like to surface-like scaling. In larger particles, the spherulites deep inside the particle have more time to grow, and if the particle is large enough, they make contact and form a compact object resisting degradation. In the extreme case only an outer layer of the particle is degraded, which we see as the quadratic scaling $\propto R_{h0}^2$ in the figure. In smaller particles the spherulites have not enough time to fill space densely, and the amorphous matrix between them is (partly) degraded. We then see a volume-like scaling $\propto R_{h0}^3$.

The bottom panel of figure 15 depicts how long the degradation process takes, defined as the time when the degradation and the growth curves approach each other closer than 5% for the first time. For large particles, this time seems to converge towards a constant value, around 2.3h. This is in accordance with the idea that only an outer layer of the particle is degraded, leaving a compact object of spherulites. The thickness of the layer is then around 32μm, which explains why at the left side

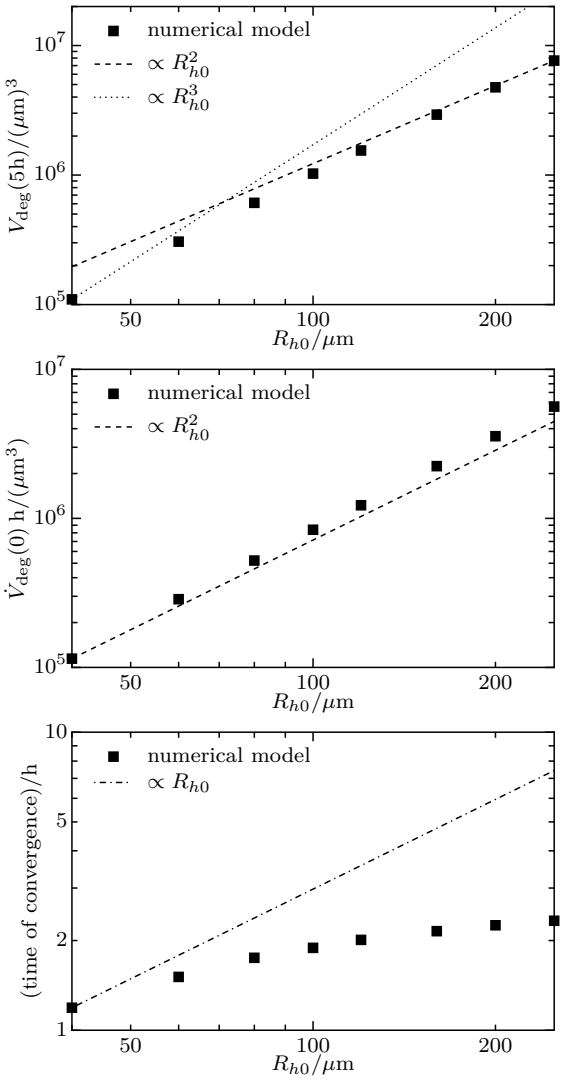

Figure 15. The effect of particle size: Numerical solution of the model, applied to PET particles from textiles, treated at 75°C. Shown are three chosen quantifiers for the yield of monomers, as a function of the parameter R_{h0}. All other parameters are constant as given in tables (12) and (16).

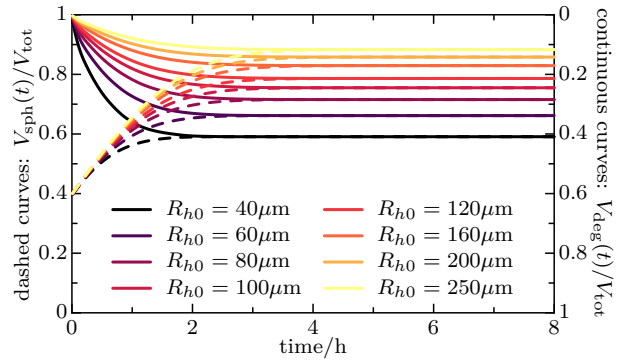

Figure 16. Time-dependent solutions of the model, same as in figure 15.

of the plot the data cross over to linear scaling, in which the particle is (partly) degraded down to its center.

Instead of showing the absolute degraded volume, it might be more interesting to see what percentage of a given material one might obtain, depending on how finely it is milled. In principle, this information is read off the top panel of figure 15, when comparing the data points with the line $\propto R_{h0}^3$. Figure 16 shows this information more conveniently, by rescaling the evolving volumes by the total initial volume of the particle. The data points in figure 15 were obtained from the curves in figure 16. Clearly, small particles are degraded more quickly, and to a higher fraction.

VI. SUMMARY

Plastic particles from waste sources are usually heterogeneous, comprising an amorphous matrix which is degradable by enzymes, and recalcitrant spherulites embedded in the matrix. Because of the thermal treatment before exposing the particles to enzymes, the heterogeneity evolves in time. We present a model for these combined dynamics, which accounts for both the degradation of the amorphous matrix and the growth of embedded spherulites.

The core of the model is that we treat the degrading particle and the spherulites as spheres whose radii change in time. We thereby convert the combined growth/degradation problem into a geometrical problem. The spherulites can overlap, and they can stick out of the degrading particle. In the latter case the spherulites block enzymes from accessing the amorphous matrix and thus influence the rate at which amorphous material is degraded. The overlap of spherulites places our model in the class of Avrami models. Here, the spherulite growth is further limited by the shrinking amorphous particle. There is thus a mutual influence of spherulite growth and degradation of amorphous matrix.

We thus cannot use the simple exponential Avrami function (8) to describe the spherulite volume as a function of time. The finite size of the degrading particle breaks the assumptions underlying the derivation and the validity of the simple exponential Avrami function. Instead of trying to derive an alternative Avrami function, we solve the model equations (1)–(5) which operate on an explicit finite set of spherulites at given positions.

In section III we present a new numerical algorithm to solve the model equations and to calculate all required geometrical quantities. The core of the algorithm is to extend a Voronoi tessellation to a double tessellation, which covers the degrading particle twice.

In section IV we show how to obtain the model parameters from experimental data. This is done for two different materials, each degraded at different temperatures. We find that the mapping between model and experiment works very well for particles obtained from PET textile waste, and it works to an acceptable degree for those taken from PET bottle waste.

In section V we use the model to make predictions for the result of degradation for parameters that we did not vary in the experiments. In particular, the initial crystallinity (more precisely the volume fraction of spherulites) has an important influence on the final yield of monomers obtained.

We further use our model to render evident that the initial crystallinity and volume fraction of spherulites is quite an ambiguous quantity and in general does not allow to predict the outcome of degradation processes. The same overall volume can be split into many small or few big spherulites, and their number impacts their distances from each other, and thus together with their growth rate also the time when they will form a compact recalcitrant object. We elucidate this idea first on conceptual parameters in figure 6 and then again in figure 14 with the parameters taken from experiments.

From the numerical solution of the model we extract selected quantifiers, namely the obtained yield after some given time (e.g. five hours), the initial rate of yield, and the time when the process finishes. We find that the initial rate of degradation is actually no indicator for the final yield of degradation as it depends on both the size of the particle and on the size and volume fraction of the internal spherulites.

We further use our model to make a prediction for the influence of the particle size on the yield. We find two regimes, in the first small particles are degraded to their center, and in the second large particles have only an outer shell degraded. We can quantify the crossover between these two regimes, as well as the thickness of the outer layer.

[1] V. Tournier, C. M. Topham, A. Gilles, B. David, C. Folgoas, E. Moya-Leclair, E. Kamionka, M.-L. Desrousseaux, H. Texier, S. Gavalda, M. Cot, E. Guémard, M. Dalibey, J. Nomme, G. Cioci, S. Barbe, M. Chateau, I. André, S. Duquesne, and A. Marty, An engineered PET depolymerase to break down and recycle plastic bottles, Nature **580**, 216 (2020).

[2] R. Wei, G. von Haugwitz, L. Pfaff, J. Mican, C. P. S. Badenhorst, W. Liu, G. Weber, H. P. Austin, D. Bednar, J. Damborsky, and U. T. Bornscheuer, Mechanism-based design of efficient PET hydrolases, ACS Catalysis **12**, 3382 (2022).

[3] A. Singh, N. A. Rorrer, S. R. Nicholson, E. Erickson, J. S. DesVeaux, A. F. Avelino, P. Lamers, A. Bhatt, Y. Zhang,

G. Avery, L. Tao, A. R. Pickford, A. C. Carpenter, J. E. McGeehan, and G. T. Beckham, Techno-economic, lifecycle, and socioeconomic impact analysis of enzymatic recycling of poly(ethylene terephthalate), Joule **5**, 2479 (2021).

[4] L. T. J. Korley, T. H. Epps, B. A. Helms, and A. J. Ryan, Toward polymer upcycling—adding value and tackling circularity, Science **373**, 66 (2021).

[5] V. Tournier, S. Duquesne, F. Guillamot, H. Cramail, D. Taton, A. Marty, and I. André, Enzymes' power for plastics degradation, Chemical Reviews **123**, 5612 (2023).

[6] F. Kawai, R. Iizuka, and T. Kawabata, Engineered polyethylene terephthalate hydrolases: Perspectives and limits, Applied Microbiology and Biotechnology **108**, 404 (2024).

[7] A. Zaker and K. Auclair, Impact of ball milling on the microstructure of polyethylene terephthalate, ChemSusChem **18**, e202401506 (2025).

[8] M. Ley-Flores, A. Chabbi, R. Alessandri, S. Marsden, I. Vettese, S. J. Rowan, and J. J. de Pablo, Numerical study of cleavable bond-modified polyethylene for circular polymer design, arXiv cond-mat.soft , 2404.09341 (2024).

[9] G. Arnal, J. Anglade, S. Gavalda, V. Tournier, N. Chabot, U. T. Bornscheuer, G. Weber, and A. Marty, Assessment of four engineered PET degrading enzymes considering large-scale industrial applications, ACS Catalysis **13**, 13156 (2023).

[10] Y. Cui, Y. Chen, J. Sun, C. Li, W.-C. Geng, and B. Wu, Computational redesign of a hydrolase for nearly complete PET depolymerization at industrially relevant high-solids loading, Nature Communications **15**, 1417 (2024).

[11] E. L. Bell, G. Rosetto, M. A. Ingraham, K. J. Ramirez, C. Lincoln, R. W. Clarke, J. E. Gado, J. L. Lilly, K. H. Kucharzy, E. Erickson, and G. T. Beckham, Natural diversity screening, assay development, and characterization of nylon-6 enzymatic depolymerization, Nature Communications **15**, 1217 (2024).

[12] J. Benninga, J. Jager, R. Folkersma, V. S. D. Voet, and K. Loos, Enzymatic recycling of polyurethanes, in *Sustainable Green Chemistry in Polymer Research. Volume 1. Biocatalysis and Biobased Materials*, ACS Symposium Series No. 1450, edited by H. N. Cheng and R. A. Gross (American Chemical Society, 2023) Chap. 5, pp. 71–87.

[13] X.-F. Wei, A. J. Capezza, Y. Cui, L. Li, A. Hakonen, B. Liu, and M. S. Hedenqvist, Millions of microplastics released from a biodegradable polymer during biodegradation/enzymatic hydrolysis, Water Research **211**, 118068 (2022).

[14] B. C. Almeida, P. Figueiredo, and A. T. P. Carvalho, Polycaprolactone enzymatic hydrolysis: A mechanistic study, ACS Omega **4**, 6769 (2019).

[15] V. Perz, M. T. Zumstein, M. Sander, S. Zitzenbacher, D. Ribitsch, and G. M. Guebitz, Biomimetic approach to enhance enzymatic hydrolysis of the synthetic polyester poly(1,4-butylene adipate): Fusing binding modules to esterases, Biomacromolecules **16**, 3889 (2015).

[16] K. Welzel, *Einfluss der chemischen Struktur auf die enzymatische Hydrolyse von Polyester-Nanopartikeln*, Ph.D. thesis, Gemeinsame Naturwissenschaftliche Fakultät der Technischen Universität Carola–Wilhemina zu Braunschweig, Braunschweig (2003).

[17] G. Strobl, *The Physics of Polymers: Concepts for Understanding Their Structures and Behavior*, 3rd ed. (Springer, 2007).

[18] N. M. Nurazzi, M. N. F. Norrrahim, S. S. Shazleen, M. M. Harussani, F. A. Sabaruddin, and M. R. M. Asyraf, Introduction to polymer crystallization, in *Polymer Crystallization* (John Wiley & Sons, Ltd, 2023) Chap. 1, pp. 1–12.

[19] H. E. H. Meijer, L. E. Govaert, and T. A. P. Engels, Predicting mechanical performance of polymers, in *Macromolecular Engineering*, edited by K. Matyjaszewski, Y. Gnanou, and L. Leibler (John Wiley & Sons, Ltd, 2007) Chap. 11, pp. 1783–1825.

[20] M. Safandowska, C. Makarewicz, A. Rozanski, and R. Idczak, Barrier properties of semicrystalline polylactide: The role of crystallinity and processing, Macromolecules **55**, 10077 (2022).

[21] F. Kawai, T. Kawabata, and O. M., Current knowledge on enzymatic PET degradation and its possible application to waste stream management and other fields, Applied Microbiology & Biotechnology **103**, 4253 (2019).

[22] H. Garate, C. Freymond, L. Breloy, M. Schindler, J. Pallis, B. Gibbs, B. Mansaku, Y. Rondelez, C. Creton, A. D. Griffiths, and L. Leibler, Reactive mixing enables enzymatic depolymerization of recalcitrant or unsortable polyester wastes, Proceedings of the National Academy of Sciences **122**, e2505611122 (2025).

[23] F. van Antwerpen and D. W. van Krevelen, Influence of crystallization temperature, molecular weight, and additives on the crystallization kinetics of poly(ethylene terephthalate), Journal of polymer science **10**, 2423 (1972).

[24] T. B. Thomsen, C. J. Hunt, and A. S. Meyer, Influence of substrate crystallinity and glass transition temperature on enzymatic degradation of polyethylene terephthalate (PET), New Biotechnology **69**, 28 (2022).

[25] T. B. Thomsen, C. J. Hunt, and A. S. Meyer, Standardized method for controlled modification of poly(ethylene terephthalate) (PET) crystallinity for assaying PET degrading enzymes, MethodsX **9**, 101815 (2022).

[26] T. B. Thomsen, K. Almdal, and A. S. Meyer, Significance of poly(ethylene terephthalate) (PET) substrate crystallinity on enzymatic degradation, New Biotechnology **78**, 162 (2023).

[27] S. Weinberger, K. Haernvall, D. Scaini, G. Ghazaryan, M. T. Zumstein, M. Sander, A. Pellis, and G. M. Guebitza, Enzymatic surface hydrolysis of poly(ethylene furanoate) thin films of various crystallinities, Green Chemistry **19**, 5381 (2017).

[28] Å. M. Ronkvist, W. Xie, W. Lu, and R. A. Gross, Cutinase-catalyzed hydrolysis of poly(ethylene terephthalate), Macromolecules **42**, 5128 (2009).

[29] A. Patel, A. C. Chang, S. Perry, Y.-H. V. Soong, C. Ayafor, H.-W. Wong, D. Xie, and M. J. Sobkowicz, Melt processing pretreatment effects on enzymatic depolymerization of poly(ethylene terephthalate), ACS Sustainable Chemistry & Engineering **10**, 13619 (2022).

[30] R. Wei, D. Breite, C. Song, D. Gräsing, T. Ploss, P. Hille, R. Schwerdtfeger, J. Matysik, A. Schulze, and W. Zimmermann, Biocatalytic degradation efficiency of postconsumer polyethylene terephthalate packaging determined by their polymer microstructures, Advanced Science **6**, 1900491 (2019).

[31] T. Gaillard, M. George, E. Gastaldi, F. Nallet, and P. Fabre, An experimental and theoretical study of the

erosion of semi-crystalline polymers and the subsequent generation of microparticles, Soft Matter **15**, 8302 (2019).
[32] E. Akram, Y. Cao, H. Xing, Y. Ding, Y. Luo, R. Wei, and Y. Zhang, On the temperature dependence of enzymatic degradation of poly(ethylene terephthalate), Chinese Journal of Catalysis **60**, 284 (2024).
[33] A. Patel, A. C. Chang, A. Mastromonaco, M. A. Diaz, S. Perry, O. Ferki, C. Ayafor, U. Abid, H.-W. Wong, D. Xie, and M. J. Sobkowicz, Aqueous buffer solution-induced crystallization competes with enzymatic depolymerization of pre-treated post-consumer poly (ethylene terephthalate) waste, Polymer **285**, 126370 (2023).
[34] M. Avrami, Kinetics of phase change. I. general theory, Journal of Chemical Physics **7**, 1103 (1939).
[35] K. Shirzad and C. Viney, A critical review on applications of the Avrami equation beyond materials science, Journal of the Royal Society: Interface **20**, 20230242 (2023).
[36] M. Ye, X. Wang, W. Huang, J. Hu, and H. Bu, Fast crystallization of poly(ethylene terephthalate), Journal of Thermal Analysis **46**, 905 (1996).
[37] D. Wang, F. Luo, Z. Shen, X. Wuab, and Y. Qi, A study on the crystallization behavior and mechanical properties of poly(ethylene terephthalate) induced by chemical degradation nucleation, RSC Advances **7**, 37139 (2017).
[38] L. Corté and L. Leibler, A model for toughening of semicrystalline polymers, Macromolecules **40**, 5606 (2007).
[39] S. Wu, A generalized criterion for rubber toughening: The critical matrix ligament thickness, Journal of Applied Polymer Science **35**, 549 (1988).
[40] H. Edelsbrunner and R. Seidel, Voronoi diagrams and arrangements, Discrete & Computational Geometry **1**, 25 (1986).
[41] C. Jamin, S. Pion, and M. Teillaud, 3D triangulations, in *CGAL User and Reference Manual* (CGAL Editorial Board, 2024) 6.0.1 ed., `https://doc.cgal.org/6.0.1/Manual/packages.html#PkgTriangulation3`.
[42] M. Schindler and A. C. Maggs, Cavity averages for hard spheres in the presence of polydispersity and incomplete data, Eur. Phys. J. E **38**, 97 (2015).
[43] F. Aurenhammer, Voronoi diagrams–A survey of a fundamental geometric data structure, ACM Computing Surveys **23**, 345 (1991).
[44] H. Edelsbrunner and N. R. Shah, Incremental topological flipping works for regular triangulations, Algorithmica **15**, 223 (1996).
[45] M. Maiti, A. Lakshminarayanan, and S. Sastry, Characterization of void space in polydisperse sphere packings: Applications to hard-sphere packings and to protein structure analysis, Eur. Phys. J. E **36**, 5 (2013).
[46] S. Sastry, D. S. Corti, P. G. Debenedetti, and F. H. Stillinger, Statistical geometry of particle packings. I. Algorithm for exact determination of connectivity, volume, and surface areas of void space in monodisperse and polydisperse sphere packings, Physical Review E **56**, 5524 (1997).
[47] M. L. Di Lorenzo, Crystallization of poly(ethylene terephthalate): A review, Polymers **16**, 1 (2024).
[48] B. Wunderlich, Reversible crystallization and the rigid amorphous phase in semicrystalline macromolecules, Prog. Polym. Sci. **28**, 383 (2003).
[49] S. A. Jabarin, Optical properties of thermally crystallized poly(ethylene terephthalate), Polymer engineering and science **22**, 815 (1982).
[50] H. Seo, H. Hong, J. Park, S. H. L. Lee, D. Ki, A. Ryu, H.-Y. Sagong, and K.-J. Kim, Landscape profiling of PET depolymerases using a natural sequence cluster framework, Science **387**, eadp5637 (2025).

ACKNOWLEDGMENTS

The authors thank Costantino Creton, Andrew Griffiths, Yannick Rondelez, Matthieu Labousse, and Brian Mansaku for valuable discussions.